

## A New Inhibitor for Steel Rebar Corrosion in Concrete: Electrochemical and Theoretical Studies

Youcef Bellal<sup>1</sup>, Saida Keraghel<sup>1,\*</sup>, Fatiha Benghanem<sup>1</sup>, Toukal Linda<sup>1</sup>, Gökmen Sığırcık<sup>2</sup>,  
Bourzami Riadh<sup>3</sup>, Ali Ourari<sup>1</sup>

<sup>1</sup> Laboratory of Electrochemistry, Molecular Engineering and Redox Catalysis (LEIMCR)  
Department of Engineering Process, Faculty of Technology, Ferhat Abbas University Setif-1, Setif,  
Algeria

<sup>2</sup> Chemistry Department, Faculty of Science and Letters, Çukurova University, Adana, Turkey

<sup>3</sup> Emerging Materials Research Unit, Ferhat Abbas University Setif -1, Setif, Algeria

\*E-mail: [s\\_marouani20012002@yahoo.fr](mailto:s_marouani20012002@yahoo.fr)

Received: 11 March 2018 / Accepted: 18 April 2018 / Published: 5 June 2018

---

An original Schiff base 4-hydroxy-3-[1-(3-hydroxy-naphthalen-2-ylimino)-ethyl]-6-methyl-pyran-2-one (L<sub>1</sub>) is synthesized using the condensation method and characterized by X-ray diffraction spectroscopy (XRD). The compound obtained is a mono-crystal. The study of its inhibitory efficiency with respect to the corrosion of mild steel in reinforced concrete was realized using the potentiodynamic polarization and impedance spectroscopy (EIS) as electrochemical methods. The inhibition power of this Schiff base against the corrosion of mild steel in concrete is studied in the aggressive medium 0.5M NaCl as a function of the concentration of the inhibitor, immersion time and temperature. High inhibition power 90% is determined for the low concentration 10<sup>-6</sup>M at t=28 days and T= 30°C. This inhibition increases as a function of temperature. The thermodynamic study was used to identify the mechanism of inhibitory action of L<sub>1</sub>. The inhibiting power (EI%) and the apparent activation energy (E<sub>a</sub>) have been calculated at different concentrations of L<sub>1</sub>. The values of  $\Delta G_{ads}$ , E<sub>a</sub>,  $\Delta H_a$ , and  $\Delta S_a$  showed that L<sub>1</sub> is a good inhibitor of corrosion of the rebar in concrete in an environment of 0.5M NaCl. The inhibitor studied follows a chemisorption process. The adsorption behavior of this product obeys to Langmuir isotherm. The electrochemical results were confirmed with scanning electron microscopy (SEM). The quantum chemical parameters determined by theoretical calculations were used to elucidate the relationship between inhibiting effect of L<sub>1</sub> and its molecular structure.

---

**Keywords:** Corrosion, Concrete, Inhibitor, Schiff bases, XRD, EIS, SEM, DFT.

### 1. INTRODUCTION

Corrosion of concrete rebar is one of the principal factors limiting the lifetime of reinforced concrete buildings [1-3]. The use of inhibitors remains a very easy and effective means to protect the

rebar against the deterioration. Several organic species, containing elements such as nitrogen, oxygen and sulfur, also the aromatic ring in their structures which facilitate their adsorption on the metallic surface [4-6] were mostly used. The factors influencing the inhibitor effectiveness were notably electron-attraction or electron-donor effect, electrostatic effect, steric effect, and lateral interaction effect. Organic inhibitors mainly used to protect rebar towards the corrosion in concrete were specially the organic and polymer based substances as amines, alkanolamines, aminoacids, amines salts, emulsified mixtures of esters, alcohols, and carboxylates substances [1, 7]. The beneficial effect of the use of this kind of inhibitors is the ability of these compounds to block the pores in the microstructure of concrete. A monomolecular film is then formed and protects the metal surface. In this fact the diffusion process of chloride becomes difficult and the diffuse layer resistance increases [8-10]. S. Swada and coll. [11] studied two organic compounds: ethanolamine and guanidine. They concluded that the carbonation of concrete influences the efficiency of the inhibitor. The pH of the pore solution influences the degrees of ionization of these bases besides their power to migrate and their cathodic reaction with generated hydroxyl ions. The inhibiting characteristics of N,N-dimethylaminoethanol (DMEA) were evaluated in cement mortar specimens [12]. It is demonstrated that the presence of DMEA in the concrete decreases the corrosion rate. J. Kubo and coll. [13] have studied the remedial treatment by application of aqueous solutions of ethanolamine onto the concrete surface. After this electrochemical treatment, no cracks or defects were observed.

G. Mangayarkarasi and coll. [14] investigated the corrosion of steel in different types of concrete using many solutions of thiosemicarbazide, tri-ethanolamine, guanidine and ethyl acetate as electrolyte with different concentrations of chloride ions obtained by the electro injection process. The Results show that the inhibitors gave more than 95% efficiency in the different concretes. J.O. Okeniyi [15] investigated the inhibition and adsorption mechanism of  $C_{10}H_{18}N_2Na_2O_{10}$  on the rebar in concrete submerged into corrosive solutions. The electrochemical tests show that the efficiency of  $C_{10}H_{18}N_2Na_2O_{10}$  depends on its concentration. The adsorption of this inhibitor was best fitted by Langmuir isotherm indicating its chemisorption in both media. Recently, J. Abdu El Bari and coll. [7] reviewed researches on the inhibition corrosion mechanism in concrete. Many of the corrosion inhibitors of reinforcement in concrete have been briefly described with emphasis on anodic inhibitors. It is shown that the benzotriazoles have a good inhibitory effect against pitting corrosion of reinforced steel [16, 17]. Other organic compounds are studied to evaluate their inhibitive effect against corrosion of carbon steel reinforced bars embedded in carbonated Portland cement polluted with chlorides, and alkali-activated fly ash mortars [8]. The substances tested are good inhibitors in all cases. It is noticed that no laboratory investigations realized in short time could fully simulate the action of inhibitors on concrete structures in reality. U.M. Angst and coll. [18] reported the long term (18years) observations on experiences on organic corrosion inhibitors specially alkanolamines for reinforced concrete. As a result, the corrosion initiation time of the chloride-induced reinforcing steel doubles in the presence of the corrosion inhibitor. In effect, it was found that reinforced steel was free from corrosion after 18 years still, while generally the initiation of the corrosion occurs after approximately 8–9 years in the reference concrete. Other studies on the migrating organic corrosion inhibitors that have been used for more than 30 years as an economical mean of corrosion mitigation in construction were given [19]. Effectiveness has been provided on many types and ages of construction. Organic corrosion inhibitors are amine based

chemicals that have appreciable saturated vapor pressure under atmospheric conditions. This important property allows the vapor transport of these species by diffusion throughout the pores of the concrete structures to give a protective molecular layer. The organic corrosion inhibitors are found to be a mixed type. The inhibition of the cathodic reaction is reached by the admixture of one or more oxidizing radicals in the organic molecules, which are hydrolyzed and then adsorbed on the metal surface. The nitrogen atom is coordinated to the steel rebar thus improving the adsorption process. Therefore, the resistance of the metal to the corrosion increases because the pH at the interface is above 9. The type and application method of the organic corrosion inhibitors affect their migrating process through the concrete. The amine carboxylates were first introduced in the early 1990's but the amine alcohols were used before. This kind of inhibitors combined with some set retarding materials can increase the setting times, but generally no other concrete properties are affected. The significant ability to increase service life of structures with a single application of these inhibitors during construction, repair or in a novel applications was noticed [20].

At the other hand, the presence of the organic inhibitors in concrete structures affects its compressive strength. This last property of the concrete specimens with inhibitor was superior to that of the control sample [20, 21]. The elevation of the compressive strength of 19 - 24% measured for specimens containing polyvinylpyrrolidone PVP is noticed [22].

Generally it appears from the literature that the interaction mechanisms of inhibitors with protective film of the passivated steel needs further comprehension. For this aim, the quantum chemical calculations (DFT) and molecular dynamics simulations (MD) methods have been employed. The use of these techniques permits to simulate the electrochemical data and elucidate the adsorption process and explain the mechanism of corrosion inhibition in several industrial media notably in chloride-rich alkaline solution simulating the solution pore of concrete [23, 24]. Quantum chemical and molecular dynamics simulations studies on inhibition performances of some organic inhibitors against corrosion of iron are reported [25-29]. The DFT calculations show that the N=C-N region in aromatic ring is the preferential active site for the adsorption. The donor-acceptor interactions occur between the lone electron pairs on nitrogen atoms together with the  $\pi$  electrons of heterocyclic and the vacant d orbital of iron atoms. The adsorption of Schiff bases follows physicochemical mechanism. The process is spontaneous, exothermic and obeys Langmuir isotherm. The Schiff bases are a cathodic inhibitor type in NaOH. It is demonstrated that the zone containing N and O atoms are the principal sites for coordinating the metal [27].

In view of this bibliographic synthesis on the corrosion inhibition of reinforced of concrete, it appears that amines or aminoalcohols are the most used and are very promoters in the preservation of concrete structures. No study was found on the inhibition of rebars in concretes structures by Schiff bases. Also, considering that Schiff bases were largely employed in corrosion protection area and the results were very satisfactory in alkaline environments which can simulate the interface (reinforcement/concrete) [27, 30, 31], we proposed to investigate the efficiency of 4-hydroxy-3-[1-(3-hydroxy-naphthalen-2-ylimino)-ethyl]-6-methyl-pyran-2-one against the corrosion of mild steel in concrete. For this purpose, we prepared and characterized by different physicochemical methods (FT-IR and XRD) the Schiff base L<sub>1</sub>. Then we studied the inhibitory power of this Schiff base against the corrosion of ordinary steel in concrete contaminated with 0.5M NaCl. Potentiodynamic polarization and

EIS methods were used in this study. The SEM technique was carried out to confirm inhibitory behavior of L<sub>1</sub>. The DFT was employed to determine the quantum chemical parameters, to elucidate the adsorption behavior and to propose the mechanism of corrosion inhibition in concrete. Mechanical tests were realized to examine the influence of inhibitor on compressive strength of concrete reinforcement.

## 2. EXPERIMENTAL

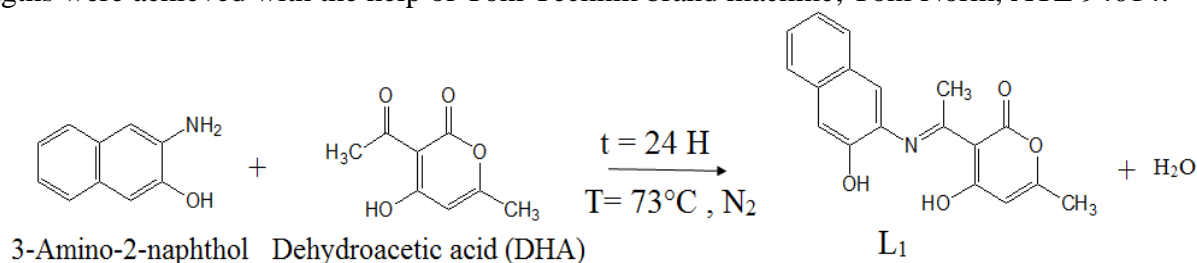
All chemical substances: 3-amino-2-naphthol, Dehydroacetic Acid (DHA), and solvents were analytical grade Aldrich

### 2.1. Synthesis of L<sub>1</sub>

The synthesis of the non-symmetrical tridentate Schiff base L<sub>1</sub> was performed by a reaction of 1 mmole of dehydroacetic acid (DHA) (168.15 mg) dissolved in 10 ml of absolute methanol with 1 mmole of 3-amino-2-naphthol (159.19 mg) dissolved in 10 ml of absolute methanol (Scheme1). The solution was stirred under nitrogen for 24 hours at T=73°C. A green precipitate was obtained three hours after the initiation of the reaction, washed with hot methanol and diethyl ether and recrystallized in the mixed solvent (DMSO/CH<sub>3</sub>CN) (V<sub>DMSO</sub>=1/5 V<sub>Methanol</sub>). The synthesized compound L<sub>1</sub> was purified by chromatography (TLC) using silica gel plates and dichloromethane (CH<sub>2</sub>Cl<sub>2</sub>).

m.p. 276 °C; FT-IR (KBr,  $\nu_x(\text{cm}^{-1})$ ):  $\nu_{\text{O-H}}$  (3078),  $\nu_{\text{(N-H)}}$  (2361);  $\nu_{\text{(C=O)}}$  (1695),  $\nu_{\text{(C=C)}}$  (1550-1471).

A Shimadzu 1000-FT-IR spectrometer and the standard KBr pellet technique were used to record FT-IR transmission spectra in the 4000-400cm<sup>-1</sup> range. The crystallographic structure of the ligand was determined by the Bruker SMART APEXII CCD diffractometer. The melting point for the L<sub>1</sub> was determined by the Kofler Banc 7779 apparatus. The measure of the molar conductance of the L<sub>1</sub> in CH<sub>3</sub>CN was performed by conductivity Meter MeterLab CDM-210 at room temperature. Mechanical strengths were achieved with the help of Toni Technik brand machine; Toni Norm, ATL 94014.

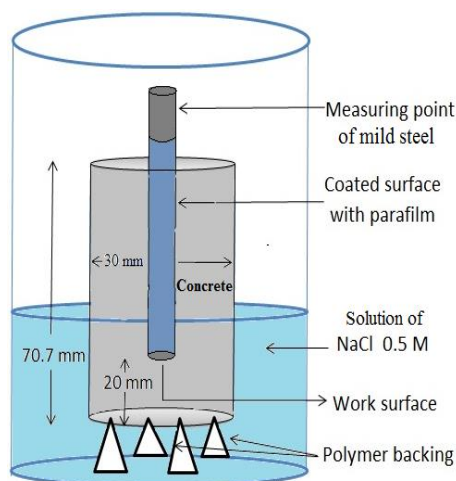


**Scheme1.** Synthesis of 4-hydroxy-3-[1-(3-hydroxy-naphthalen-2-ylimino)-ethyl]-6-methyl-pyran-2-one.

2.2. Metal specimen

**Table 1.** Chemical composition of cement.

Chemical elements	SiO <sub>2</sub>	Al <sub>2</sub> O <sub>3</sub>	Fe <sub>2</sub> O <sub>3</sub>	CaO	MgO	K <sub>2</sub> O	Na <sub>2</sub> O	SO <sub>3</sub>	Cl <sup>-</sup>	CO <sub>2</sub>
%	22.98	5.55	5.47	58.46	1.41	0.37	0.05	1.85	0.001	3.86



**Scheme 2.** Concrete specimen containing a bar of mild steel immersed in 0.5M NaCl.

In this investigation, the specimens used as working electrode were cylindrical mild steel rebars of 6mm in diameter with the following chemical composition in weight%: 97.321 Fe, 0.58 Si, 0.423 Mn, 0.079 Cr, 0.029 Mo, 0.215 Ni, 0.536 Cu, 0.013 Sn, 0.804 C. The surface of reinforcing bars was  $S = 28.26 \text{ mm}^2$ . Cylindrical concrete samples were prepared in such way to have a volume of 50 ml, i.e 30 mm in diameter and 70 mm in length. The concrete was prepared with cement as chemical composition is given in **Table 1** and the standard sand washed with distilled water conforms to ISO 679:2009 (Provided by Nouvelle du Littoral Society). The concrete is mixed with 0.1M NaOH solution containing different concentrations of L<sub>1</sub>, sand and cement (sand quantity is three times the amount of cement). Before that, the surface of specimen steel were polished with 350-2000 grades wet SiC papers, rinsed with acetone then with distilled water. The periphery of the steel bar is enrobed with the parafilm before immersing it in the concrete (**Scheme 2**). The distance between a rebar and the bottom of the concrete is equal to 20 mm. The samples were placed individually in their aggressive medium 0.5M NaCl. The electrochemical tests carried out on the samples at t=2, 7, 14, 21 and 28 days. The temperature is varied from 30 to 60°C.

2.3. Electrochemical measurements

The electrochemical analysis was conducted using a mild steel enrobed with concrete like working electrode (WE), platinum plate ( $S = 10 \text{ mm}^2$ ) as auxiliary electrode (AE) and the system

(Hg/Hg<sub>2</sub>Cl<sub>2</sub>/KCl) as reference electrode (RE). The experiments were carried out in thermostatted cell. The electrochemical measurements were recorded using a VOLTALAB PGZ 301. The "Voltmaster 4" software was used to analyze the experimental results. Before starting and recording the polarization curves, an open circuit potential (OCP) is maintained for 30 minutes until reaching a steady state. The EIS measurements were performed at open circuit potential (OCP) within the frequency range from 100kHz to 5mHz with 10 points per decade. In potentiodynamic polarization mode the cathodic branch was recorded at first. Then, the anodic branch was determined after establishing the open-circuit potential. The sweep rate of potential is equal to 2 mV.s<sup>-1</sup>. The exploitation and plotting of the Tafel curves were used to determine the various electrochemical characteristics (corrosion potential ( $E_{\text{corr}}$ ), corrosion current density ( $i_{\text{corr}}$ ), polarization resistance ( $R_p$ ), corrosion rate ( $\tau_{\text{corr}}$ ) then the inhibition efficiency EI(%) from the following relation

$$EI(\%) = \frac{i_{\text{corr}} - i_{\text{corr(inh)}}}{i_{\text{corr}}} \times 100 \quad (1)$$

where  $i_{\text{corr}}$  and  $i_{\text{corr(inh)}}$  are the corrosion current density values without and with inhibitor, respectively, obtained by intersecting the corrosion potential and the anodic and cathodic slopes of Tafel lines. The polarization resistance ( $R_p$ ) and the double layer capacitance ( $C_{\text{dl}}$ ) were determined from Nyquist plots using the half-circle fit.

#### 2.4. Theoretical calculations

The theoretical calculations were given by the DFT method (at B3LYP) functional with 6-31 G (d,p) basis set for all atoms in the gas and aqueous phases [32, 33]. The geometry of the prepared compound structure was optimized by the standard Gaussian 09W software package [34, 35]. The absolute electronegativity ( $\chi$ ), electrophilicity index ( $\omega$ ), dipole moment ( $\mu$ ), global hardness ( $\eta$ ) and softness ( $\sigma$ ), electron affinity (A), ionization potential (I), gap energy ( $\Delta E$ ), and the number of transferred electron ( $\Delta N$ ) were determined using the following equations:

$$\chi = (I + A)/2 \quad (2)$$

$$\eta = (I - A)/2 \quad (3)$$

where I and A are related to the frontier orbital energies according to equations (4) and (5):

$$I = -E_{\text{HOMO}} \quad (4)$$

$$A = -E_{\text{LUMO}} \quad (5)$$

deduced from Koopmans' theory [36].

The values of  $\chi$  and  $\eta$  for L<sub>1</sub> obtained using the values of I and A permit to calculate the number of transferred electrons ( $\Delta N$ ) using the following equation:

$$\Delta N = (\chi_{\text{Fe}} - \chi_{\text{Inh}})/2(\eta_{\text{Fe}} + \eta_{\text{Inh}}) \quad (6)$$

Where  $\chi_{\text{Fe}}$  and  $\chi_{\text{Inh}}$  are the absolute electronegativities of iron and inhibitor, and  $\eta_{\text{Fe}}$  and  $\eta_{\text{Inh}}$  are the absolute hardnesses of iron and the inhibitor respectively. From the literature [37, 38], the  $\chi$  and  $\eta$  theoretical values for iron are equal to 7.0eVmol<sup>-1</sup> and 0eVmol<sup>-1</sup> respectively.

From the following equations, the softness ( $\sigma$ ) and the electrophilicity index ( $\omega$ ) were calculated:

$$\sigma = 1/\eta \quad (7)$$

$$\omega = \chi^2/2\eta \tag{8}$$

### 2.5. Solution and general conditions for mechanical measurements

The specimens are made only with concrete and without mild steel to see the influence of the addition of the NaOH 0.1M and inhibitor L<sub>1</sub> on the mechanical strength of the concrete. We have used different concentrations of L<sub>1</sub>. The specimens have a parallelepiped shape with volume V = L x l x h (V= 160x40x40 (mm<sup>3</sup>)). The samples were post-cured for 24 hours and then placed individually in their external aggressive solution 0.5M NaCl. The mechanical tests were carried out on the samples at t=2, 28 and 90 days keeping the temperature constant T=30°C in climate chamber. The samples were prepared in the laboratory of Ain El Kebira Setif Algeria.

## 3. RESULTS AND DISCUSSION

### 3.1. Molar conductivity measurements

The molar conductivity measured at T = 19.7 °C for C<sub>L1</sub> = 10<sup>-3</sup>M in 5 ml of the acetonitrile is equal to Λ = 13.72 Ω<sup>-1</sup>cm<sup>2</sup>mol<sup>-1</sup>. This value indicates that L<sub>1</sub> is not an electrolyte [39, 40].

### 3.2. Spectral studies

#### 3.2.1. Infrared spectra

From the FT-IR spectra recorded for L<sub>1</sub> (**Fig.1**), it appears that the ν<sub>O-H</sub> hydroxyl groups of the L<sub>1</sub> appear at 3078cm<sup>-1</sup> [41]. This frequency is due to the inter- and intra-molecular interactions or hydrogen bonds. A strong absorption band, noted at 2361cm<sup>-1</sup> expressed the N-H stretching vibration and another observed at 1695cm<sup>-1</sup>, is attributed to C=O (carbonyl) stretching vibration [42, 43]. The ν<sub>C=C</sub> vibrational frequencies are shown at 1550 and 1471cm<sup>-1</sup> [42, 44]

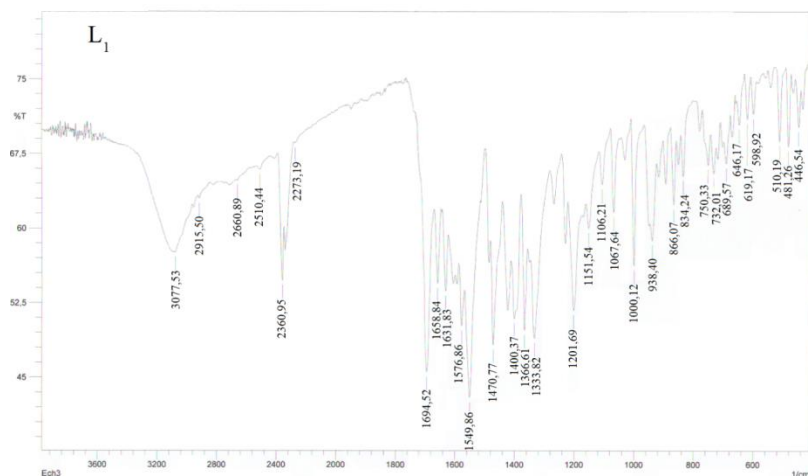
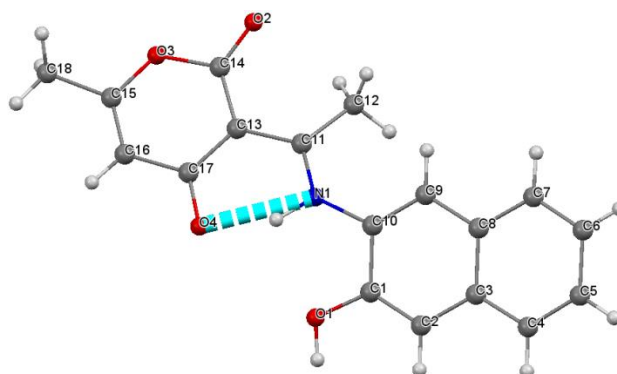


Figure 1. Infrared spectra of L<sub>1</sub>

## 3.2.2. Crystal structure

**Table 2.** Crystallographic, refinement and collection data of L<sub>1</sub>.

Molecular formula	C <sub>18</sub> H <sub>15</sub> NO <sub>4</sub>
Molecular weight (g/mol)	309.31
Temperature (K)	173(2)
Radiation	MoK $\alpha$ ( $\lambda=0.71073$ Å )
Crystal system	Monoclinic
Space group	P 2 <sub>1</sub> /c
a (Å)	13.6649(6)
b (Å)	7.2010(2)
c (Å)	14.5552(5)
$\beta$ (°)	94.844(2)
Volume (Å <sup>3</sup> )	1427.13(9)
Z	4
D <sub>calc</sub> (g.cm <sup>-3</sup> )	1.440
Crystal size (mm <sup>3</sup> )	0.50*0.40*0.35
Crystal description	prism
Crystal colour	pale yellow
Absorption coefficient (mm <sup>-1</sup> )	0.103
F (000)	648
Reflections collected/unique	8340/3256 [R av R <sub>eq</sub> =0.0683]
Range/indices (h,k,l)	-16→17; -9→8; -14→18
Teta <sub>limit</sub> (°)	1.0→27.5
No. of observed data, I > 2 sigma(I)	2678
No. of variables	218
No. of restraints	0
Goodness of fit on F <sup>2</sup>	1.071
Largest diff. Peak and hole (eÅ <sup>-3</sup> )	0.331 and -0.295
R <sub>1</sub> ,wR <sub>2</sub> [I ≥ 2 sigma(I)] <sup>a</sup>	0.0469, 0.1326
R <sub>1</sub> ,wR <sub>2</sub> (all data) <sup>a</sup>	0.0589, 0.1475

**Figure 2.** Intramolecular hydrogen-bond in asymmetric unit of L<sub>1</sub> with atom numbering.

**Table 3.** Selected bond lengths (Å) and angle (°) of L<sub>1</sub>.

Bond lengths (Å)		Bond angles (°)	
C1-O1	1.35 (16)	O1-C1-C2	124.78(12)
C1-C10	1.43 (19)	O1-C1-C10	114.78(12)
C11-N1	1.33 (17)	C9-C10-N1	125.87(12)
C11-C13	1.43 (19)	N1-C10-C1	114.07(11)
C15-C16	1.33 (2)	N1-C11-C13	117.07(12)
C10-N1	1.42 (17)	N1-C11-C12	119.41(12)
C11-C12	1.49 (19)	C13-C11-C12	123.39(12)
C14-O2	1.21 (18)	C11-C13-C17	121.38(12)
C14-O3	1.40 (17)	C11-C13-C14	119.31(12)
C15-O3	1.36 (18)	C17-C13-C14	119.27(13)
C17-O4	1.27 (17)	O2-C14-O3	113.98(13)
N1-H1	0.96 (19)	O2-C14-C13	128.46(14)
O1-H1	0.91(2)	O3-C14-C13	117.55(12)
		C16-C15-O3	122.17(13)
		O3-C15-C18	112.48(13)
		O4-C17-C16	119.02(13)
		O4-C17-C13	123.16(13)
		C11-N1-C10	131.60(12)
		C15-O3-C14	122.01(12)

The single-crystal XRD analysis has been used to identify and confirm the synthesized compound structure. The diffraction data were possessed at 173(2) K, on a Collect (Nonius B.V., 1998) diffractometer, equipped with a graphite monochromator, using fine-focus MoK $\alpha$  sealed tube as radiation source, and phi and omega scans method. The structure was resolved using SHELXS-97 (Sheldrick, 1997) program [45], while refined by SHELXL-97 (Sheldrick, 1997) [45]. The data reduction and the unit cell refinement were carried out using Denzo (Nonius B.V., 1998) [46]. All non hydrogen atoms were refined anisotropically, but the hydrogens were only included in geometric positions. The molecular graphics were computed with PLATON 98 (Spek, 1998) [47]. Table 2 presents the crystallographic data, refinement, instrumental parameters used in the unit-cell determination and data collection. Figure 2 shows the resolved asymmetric unit of L<sub>1</sub>. The L<sub>1</sub> molecule C<sub>18</sub>H<sub>15</sub>NO<sub>4</sub> refined is identical to that proposed by the spectroscopic results. It is cited in the literature for this type of molecule that they crystallises in two tautomers forms: the phenol-imine (O—H $\cdots$ N) and keto-amine (N—H $\cdots$ O) forms, and the proton-transfer reaction occurs between the phenol-imine and keto-amine tautomer [48]. The short C17—O4 and C11—C13 bonds length are 1.27(17) and 1.43(19) Å (Table 3) characterize the C=O and C=C double bonds, respectively, illustrate that this Schiff base crystallizes in the Keto-amine tautomer conformation.

Also, the C17—O4 bond distance 1.27(17) Å is perfectly compared to the corresponding distances 1.264(19) Å of (E)-6-methyl-2-oxo-3-[1-(p-tolyliminio) ethyl]-2H-pyran-4-olate [48] and confirms the proposed structure. The C11—N1 iminium bond length 1.33(17) Å is comparable to the length values 1.324(2) and 1.312(3) Å observed in (E)-6-methyl-2-oxo-3-[1-(p-tolyliminio) ethyl]-2H-

pyran-4-olate [48], and 3-[1-(4 Bromophenylamino)ethylidene]-6-methylpyran- 2,4-dione [49] respectively, those bond length confirm that the  $L_1$  molecule has a zwitterion form with cationic iminium and anionic enolate groups. The very short C15—C16 bond 1.33(2)Å, indicates a significant quinoidal effect [50-52], implying that the  $L_1$  is photochromic at solid state [53]. The difference between the bond length values of the N1—C10 (1.42(17)Å) and the N1—C11 bond (1.33(17)Å) and the angle value of C11—N1—C10 (131.60(12)°) lead to the existence of an intra-molecular H-bond with the enolate atom and O4 (N1—H1...O4), generating an S(6) ring motif [50, 54]. This H-bond assumes the presence of carbonyl group located at C17 position and implies a significant change in the molecule's conformation.

The weak intermolecular hydrogen bonds O1—H1...O4<sup>i</sup> ((i)  $-x+1, -y, -z+1$ ) stabilize the crystal structure (Fig. 2). The table 4 resumes the H-bond in  $L_1$  with corresponding donor and acceptor bonds length.

**Table 4.** Hydrogen-bond geometry (Å,°).

D—H...A	D—H	H...A	D...A	D—H...A
O1—H1...O4 <sup>i</sup>	0.91(2)	1.74(2)	2.64(15)	166(2)
N1—H1N...O4	0.96(19)	1.65(19)	2.55(15)	153(18)

Symmetry code: (i)  $-x+1, -y, -z+1$ .

The C17—C13—C11—N1 and C13—C11—N1—C10 torsion angles are -7.2(2) and -179 (13), respectively, this indicates that the molecule is not planar and the dihedral angle between the two planes defined by O(1)—C(1)—C(2)—C(3)—C(4)—C(5)—C(6)— C(7)— C(8)— C(9)— C(10)—N(1) and C(11)—C(13)—C(14)— O(3)—C(15)—C(16)—C(17) is equal to 24.82(5)°.

The  $L_1$  unit cell is shown in figure 3. The crystal of  $L_1$  is monoclinic with P2<sub>1</sub>/c space group and the cell parameters are a=13.665(6)Å, b=7.201 (2)Å, c=14.555(5)Å and  $\beta$ =94.84 (2)°. The  $L_1$  is configured in four molecules in its crystallographic cell (Z = 4).

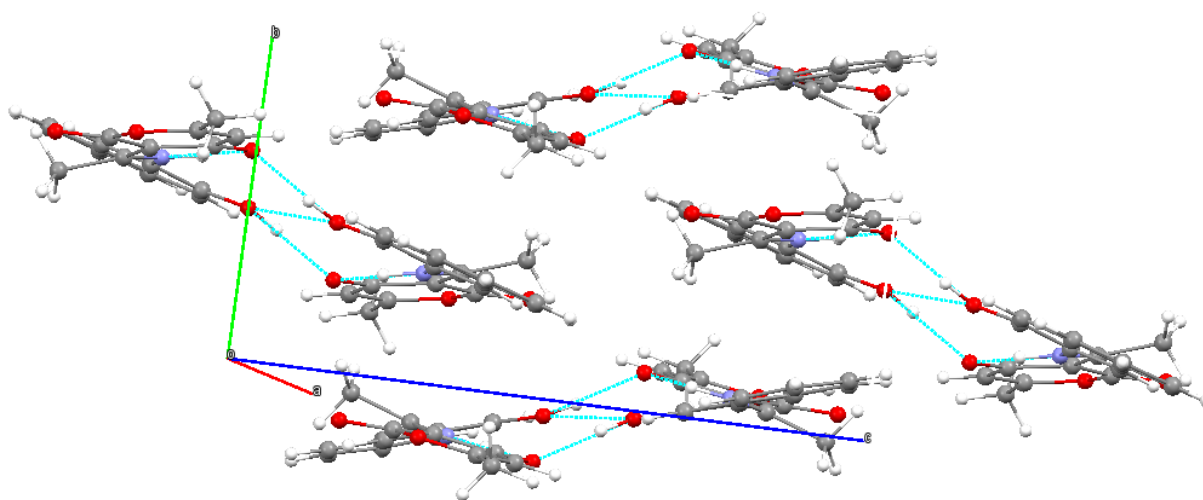


**Figure 3.** Unit cell of  $L_1$  with inter and intramolecular hydrogen bonds.

The molecules are linked into a chiral chain along c axis via O—H···O hydrogen bonds between the hydroxyl groups and the oxygen of carbonyl groups of two successive molecules (Fig. 4). The chiral chains are aligned in an antiparallel fashion forming an inversion centers in the unit cells of the crystal.

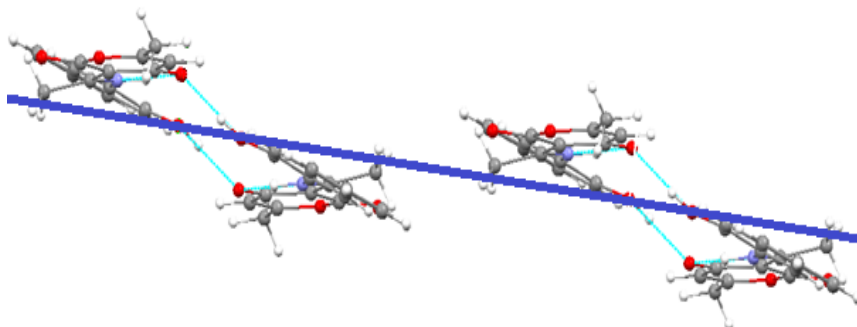


**Figure 4.** Chiral chain of  $L_1$  formed by O—H···O H-bonds.

These chiral chains offer to the  $L_1$ , a 3D corrugated network (Fig.5).

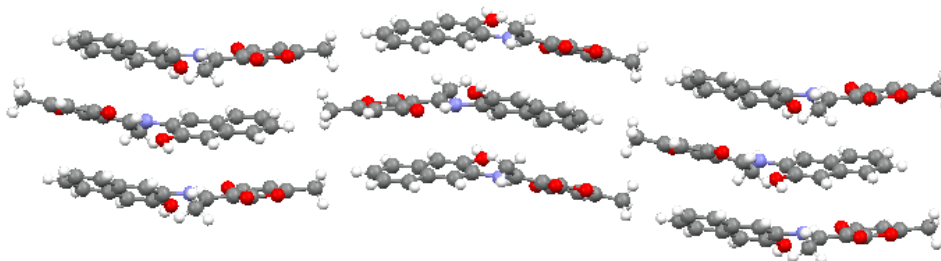


**Figure 5.** Corrugated 3D network of  $L_1$ .

The results of FT-IR spectroscopic method, elemental analysis and XRD investigations confirm the proposed structure of the  $L_1$ .

### 3.3. Electrochemical study

#### 3.3.1. Potentiodynamic polarization measurements

The inhibitory effectiveness of  $L_1$  was examined. The mechanism of the corrosion inhibition was investigated by the potentiodynamic polarization measurements. The Tafel curves for the investigated specimens immersed in 0.5M NaCl solution at various concentrations of  $L_1$  are presented in figure 6. The corrosion parameters:  $E_{\text{corr}}$ ,  $i_{\text{corr}}$ ,  $\beta_c$ ,  $\beta_a$ ,  $\tau_{\text{corr}}$  and EI(%) are determined in the concrete at different concentrations and at various immersed times.

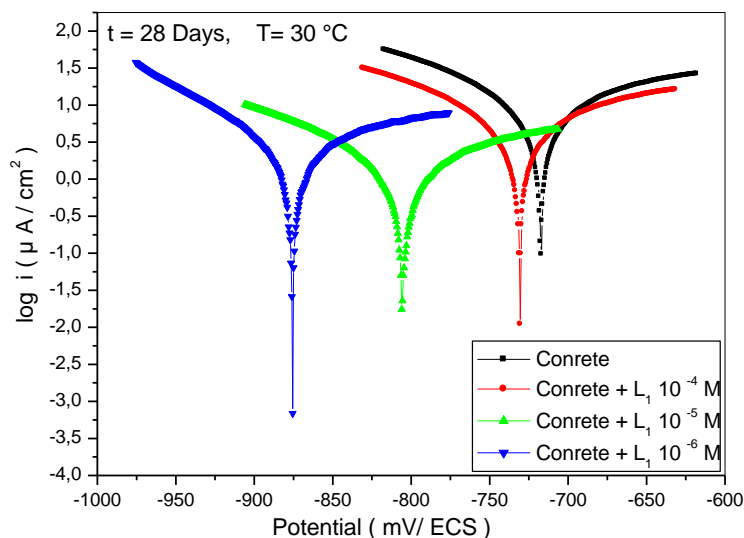


**Figure 6.** Potentiodynamic polarization curves for the corrosion of mild steel in NaCl 0,5M at different concentration of  $L_1$  at  $t = 28$  days,  $T = 30^\circ\text{C}$ .

It is observed that the presence of  $L_1$  decreases the current densities and displaces the corrosion potentials negatively. This explains that the inhibition process occurs after adsorption of  $L_1$  on the metal surface. The high inhibition power was caused by the coverage of the surface with the inhibitor molecules at low concentration involving the blocking of the metallic sites. It is noticed that the anodic and cathodic Tafel slopes increase. That implies the presence of the inhibitor retards the anodic reaction and also reduces the rate of the cathodic reduction of oxygen [31, 55]. This result can be explained by the barrier effect [55] due to the adsorbed inhibitor molecules, which causes the decrease of the cathodic transfer coefficient attributed to the thickening of the electric double layer [56]. The parallel Tafel lines (Fig.6) indicate that the inhibiting process is a charge transfer mechanism [28]. One can remark that the corrosion potential ( $E_{\text{corr}}$ ) shifts to negative values, the rate of corrosion decreases and the polarization resistance increases with the immersion time at various concentrations of  $L_1$ . This evolution of the corrosion potential as a function of time constitutes a method of monitoring the modification of the interface between the metal and its environment [31]. The electrochemical results confirm that  $L_1$  is a cathodic inhibitor as found by [28, 55]. The inhibition rate reached 84% after 28 days at  $10^{-6}\text{M}$ . This high value is due to the adsorption of  $L_1$  on the steel area. The pseudo planarity of  $L_1$  with the presence of aromatic rings explains the high effectiveness of this inhibitor [57]. The suitable anchoring sites are the nitrogen, the oxygen atoms of naphthyl and DHA groups. Their lonely  $sp^2$  electron pair and the orbitals  $p$  of the aryl rings reinforce the coordination of the  $L_1$  with the steel. This effect involves therefore the decrease of the corrosion rate due to the blocking of the active sites in the steel surface [5, 31].

3.3.2. Electrochemical impedance (EIS) measurements

As we have demonstrated previously with the potentiodynamic technique,  $L_1$  affects positively the electrochemical behavior of the mild steel in concrete immersed in the NaCl 0.5M. In order to confirm these results, the EIS method was used to explain the behaviour of the steel surface in concrete/solution interface. Figure 7 shows the dependence of the electrochemical behavior of F10 steel in 0.5M NaCl solution with the inhibitor concentration. The impedance response was significantly affected. The Nyquist plots are semicircular and their diameters increase for the low concentrations of  $L_1$ . A capacitive loop was observed at middle frequency which is related to metal/solution interface. Furthermore, the polarization resistance ( $R_p$ ) value that includes charge transfer resistance ( $R_{ct}$ ) and diffuse layer resistance ( $R_d$ ) can be obtained from the Nyquist plots. As it is clearly seen from Nyquist plot, the addition of inhibitor leads to increase of  $R_p$  values according to inhibitor free solution. However, the  $R_p$  values tend to decrease with the increase of inhibitor concentration and the opposite is right for  $C_{dl}$ . This case could be explained with the high molecular weight of  $L_1$ . Since the high molecular mass of inhibitor prevents the entrance of  $L_1$  to the steel surface, inhibitor molecules loses its efficiency at higher concentrations.

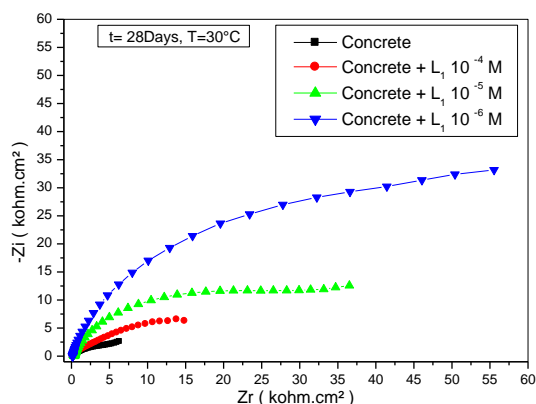


**Figure 7.** Nyquist plots for mild steel in concrete in NaCl 0.5M at different concentrations of  $L_1$  at  $t=28$ days,  $T=30^\circ\text{C}$ .

The polarization resistance values ( $R_p$ ) are determined from the difference in impedance at lower and higher frequencies. The double capacitance values ( $C_{dl}$ ) corresponding to the frequency at which the imaginary component of the impedance ( $-Z_{max}$ ) is maximum are calculated from the equation:

$$f(-Z_{max}) = \frac{1}{2\pi C_{dl} R_p} \tag{9}$$

and inhibition efficiency:

$$EI (\%) = \frac{R_{pinh} - R_p}{R_{pinh}} \times 100 \tag{10}$$

where  $R_{pinh}$  and  $R_p$  are the polarization resistance values with and without  $L_1$  respectively.

Besides,  $C_{dl}$  value is altered since adsorbed inhibitor molecules affect the interfacial charge region. The increase in  $C_{dl}$  is caused by an increase in the dielectric constant and/or an decrease in the thickness of the electric double layer, due to the adsorption of the low number of molecules of L1 [58]. These results clearly show that the dissolution of steel in 0.5M NaCl solution is limited by a charge transfer process [59]. Figure 8 illustrates, Bode plots with phase angle plots permits us to suggest an equivalent circuit containing a single constant phase element, which represents the metal/solution interface. It is seen that at low concentrations of the inhibitor, the protection is better [60].

The fitting of the obtained EIS data leads to establish the electrical equivalent circuit shown in figure 9, which represents a model for the mild steel/solution interface in the presence and absence of the inhibitor. The circuit contains  $R_s$  the electrolyte resistance,  $R_{ct}$ , the charge transfer resistance, and CPE the constant phase element [26, 61]. CPE is recommended to be used for modeling the frequency dispersion generally related to the heterogeneity of the surface. In this case the CPE replaces the double layer capacitance ( $C_{dl}$ ) in order to give a more accurate fit to the experimental results [62, 63]. The proposed circuit presents also the concrete resistance ( $R_{con}$ ) and concrete capacitance ( $C_{con}$ ).

To summarize, the obtained results from EIS method are coherent with those obtained from the other electrochemical technique used in this study.

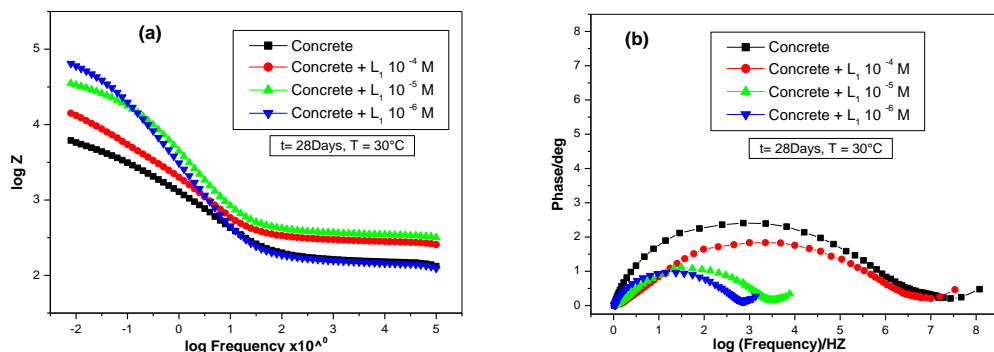


**Figure 8.** Bode plots (a) and phase angle plots (b) for mild steel in concrete in NaCl 0.5M at different concentrations of  $L_1$  at  $t= 28$ days,  $T= 30^\circ C$ .

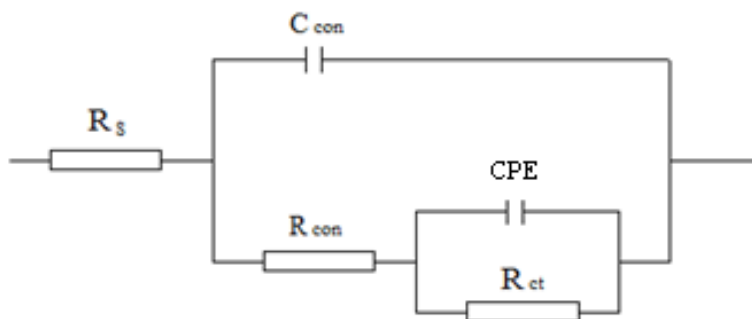


**Figure 9.** Electrochemical equivalent circuit modeling the mild steel/solution interface in the presence and absence of the inhibitor.

3.3.3. Adsorption isotherm

To determine the adsorption isotherm of L<sub>1</sub>, several isotherms were tested. The degree of surface coverage used to determine the free energy of adsorption is calculated from the potentiodynamic polarization curves using the following equations:

$$\frac{C_{inh}}{\theta} = \frac{1}{K_{ads}} + C_{inh} \tag{11} \quad \text{(Langmuir isotherm)}$$

where:  $\theta = \frac{i_{corr} - i_{corr(inh)}}{i_{corr}}$  (12)

knowing that:  $\theta$  represents the fractional surface coverage;  $C_{inh}$  is the inhibitor concentration and  $K_{ads}$  presents the equilibrium constant of the adsorption process.

The plot of  $\frac{C_{inh}}{\theta} = f(C_{inh})$  (Fig. 10), leads to evaluate  $K_{ads}$ . Then the  $\Delta G_{ads}$  was calculated with the following equation (13):

$$\Delta G_{ads} = -RT \ln (55.5 K_{ads}) \tag{13}$$

- where: **R**: Universal gas constant,  
**T**: Temperature in Kelvin K  
**55.5**: Concentration of water in solution expressed in mol/l.

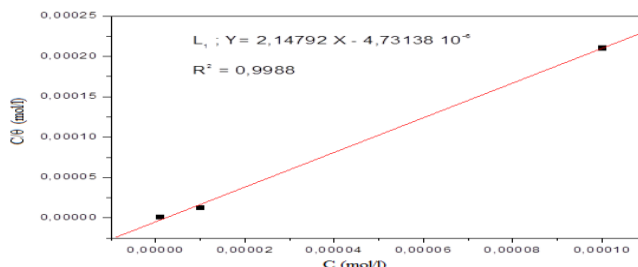


**Figure 10.** Langmuir plot for the corrosion of mild steel in concrete in NaCl 0.5M for t= 28days and T= 30°C.

A very good linear fit is obtained with a regression coefficient up to 0.9988 (Fig. 10). This provides that Langmuir isotherm is adequate for the adsorption of L<sub>1</sub> [55, 59].  $K_{ads}$  value calculated ( $K_{ads}=2.11 \cdot 10^5$ ) at T= 30°C increases with the temperature. This value agrees with the literature [15, 59].

Generally, the value of  $\Delta G_{ads} \leq -20$  KJ/mol is related to the physisorption process (electrostatic interactions between the charged molecules and the metal charge). In the case of the value of  $\Delta G_{ads} \geq -40$  KJ/mol the process follows a chemisorption ( a transfer of charges occurs between the organic molecules and the metal surface) [15, 21]. The spontaneity of the adsorption process and the stability of the adsorbed double layer on the metal area were confirmed by the negative value of  $\Delta G_{ads}$  [15]. In the present study the  $\Delta G_{ads}$  obtained value is  $-41 \text{ kJ mol}^{-1}$  at T=303K it is directly proportional to the increase of temperature (Table 5). This result proves that L1 is chemisorbed on the metal. These conclusions are in good agreement with the literature [15, 59, 64].

**Table 5.** Thermodynamics parameters for L<sub>1</sub> at different temperatures.

T(K)	K <sub>ads</sub> (mol <sup>-1</sup> )	R <sup>2</sup>	ΔG <sub>ads</sub> (kJmol <sup>-1</sup> )
303	2.11 10 <sup>5</sup>	0.9988	-41
313	2.37 10 <sup>5</sup>	0.9987	-43
323	7.34 10 <sup>5</sup>	0.9999	-47
333	8.82 10 <sup>6</sup>	1	-55

3.4. Effect of temperature

Tafel curves of corrosion of mild steel in NaCl 0.5M solution in presence of L<sub>1</sub> at the optimum concentration (10<sup>-6</sup>M) were plotted at different temperatures (Fig. 11).

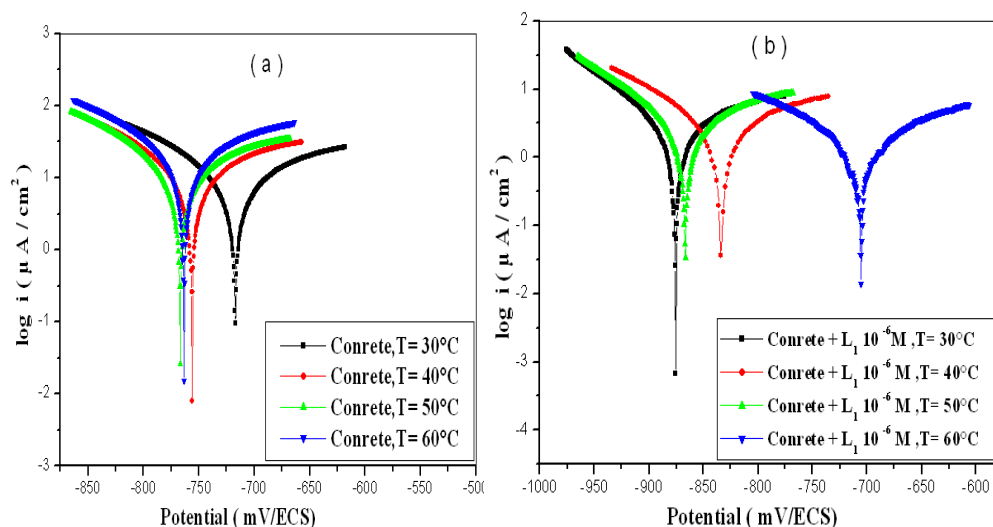


**Figure 11.** Potentiodynamic polarization curves for mild steel corrosion in 0.5M NaCl at different temperatures (a) without L<sub>1</sub>, (b) with 10<sup>-6</sup>M of L<sub>1</sub>.

When temperature varies from 30 to 50 °C the corrosion potential values shifts from -876mV/Hg/Hg<sub>2</sub>Cl<sub>2</sub> to -867mV/Hg/Hg<sub>2</sub>Cl<sub>2</sub> for 10<sup>-6</sup>M L<sub>1</sub> concentration. This could be explained by the stability of adsorbed layer even with high temperature. The corrosion potential value shifted to more positive potential for 10<sup>-6</sup>M L<sub>1</sub> concentration with respect to inhibitor free condition at 60 °C (Table 6). As it is clearly seen from this table, obtained inhibition rates are very close to each other. Moreover, inhibition efficiencies generally tended to increase with temperature. These values are high enough, 94%, for potentiodynamic and EIS results. The capacity values also decreased with increased polarization resistance values. The results obtained from both potentiodynamic and EIS methods with and without 10<sup>-6</sup>M of L<sub>1</sub> in 0,5M NaCl as a function of immersion time at T= 30°C are given in Table 7. The polarization resistances decrease with immersion time for inhibitor free condition. Besides,

inhibition efficiencies are still high enough even after 28 days immersion time, these values are 84 and 90 for potentiodynamic and EIS results, respectively.

**Table 6.** Electrochemical characteristics of mild steel in concrete with and without  $10^{-6}$ M of  $L_1$  at different temperatures in NaCl 0,5M.

Immersion Temperature (°C)	Potentiodynamic polarisation					EIS			
	Samples	$i$ ( $\mu\text{A}/\text{cm}^2$ )	$R_p$ ( $\text{k}\Omega$ )	$E$ (mV/ Hg/Hg <sub>2</sub> Cl <sub>2</sub> / KCl)	$\tau_{\text{corr}}$ ( $\mu\text{m}/\text{year}$ )	EI (%)	$R_p$ ( $\text{k}\Omega$ )	$C_{\text{dl}}$ ( $\mu\text{F}/\text{cm}$ )	EI (%)
30	Concrete	11.7	1.9	-717	137.3		7.1	925.1	
	Concrete + $10^{-6}$ M $L_1$	1.9	17	-876	29.2	84	70.8	53.2	90
40	Concrete	14.4	2	-756	168.9		8.9	606.8	
	Concrete + $10^{-6}$ M $L_1$	1.6	15	-834	36	89	31.6	102.8	72
50	Concrete	16.3	1.9	-766	191		6.3	430.8	
	Concrete + $10^{-6}$ M $L_1$	2.8	8	-867	32.7	83	31.6	174.1	80
60	Concrete	24.7	1	-764	289		2	2300	
	Concrete + $10^{-6}$ M $L_1$	1.6	13.6	-706	18.9	94	31.6	99.2	94

**Table 7.** Electrochemical characteristics of mild steel in concrete with and without  $10^{-6}$  M of  $L_1$  in NaCl 0,5M as a function of immersion times at  $T= 30^\circ\text{C}$ .

Immersion Times (Days)	Samples	Potentiodynamic polarization				Impedance (EIS)			
		$i$ ( $\mu\text{A}/\text{cm}^2$ )	$R_p$ ( $\text{k}\Omega$ )	$E$ (mV/ Hg/Hg <sub>2</sub> Cl <sub>2</sub> / KCl)	$\tau_{\text{corr}}$ ( $\mu\text{m}/\text{year}$ )	EI (%)	$R_p$ ( $\text{k}\Omega$ )	$C_{\text{dl}}$ ( $\mu\text{F}/\text{cm}^2$ )	EI (%)
2	Concrete	8.3	3.9	-687.8	97.0		3.1	91.6	
	Concrete + $10^{-6}$ M $L_1$	6.9	6.1	-813.2	80.7	17	3.8	85.4	20
7	Concrete	9.1	3.1	-743	107		26.7	812.7	
	Concrete + $10^{-6}$ M $L_1$	1.2	18.7	-792	14.1	87	128.3	52.4	80
14	Concrete	10.1	2.5	-711.7	117.2		10.1	513.9	
	Concrete + $10^{-6}$ M $L_1$	1	34.7	-798.5	11.3	91	126.6	25.3	92
21	Concrete	10.6	2.2	-770.1	122.2		10.9	637.5	

	Concrete + 10 <sup>-6</sup> M L <sub>1</sub>	5	5.8	-786.9	58.6	53	29.3	71.9	94
28	Concrete	11.7	1.9	-717.1	137.3		7.1	925.1	
	Concrete + 10 <sup>-6</sup> M L <sub>1</sub>	1.9	17	-875.6	29.1	84	70.8	53.2	90

The good inhibitor power of this compound is due to the presence of the nitrogen and the oxygen atoms and to the aryl rings in the molecular structure. It is also caused by an increase in the electron density around the adsorption sites when the temperature increases [57]. To determine the activation energy (E<sub>a</sub>), we used Arrhenius equation (14) for all cases with and without L<sub>1</sub> using the density of corrosion current determined with potentiodynamic polarization (Fig.12).

$$i_{corr} = k \exp\left(\frac{-E_a}{RT}\right) \quad (14)$$

where:

E<sub>a</sub>: Activation energy of the oxygen discharge

R: Universal gas constant

T: Temperature in degree Kevin (K)

K: Pre-exponential factor

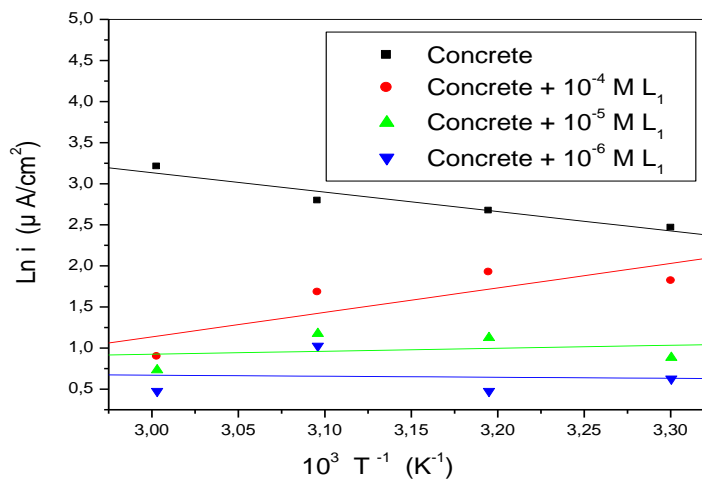


**Figure 12.**  $\ln(i_{corr}) = f(T^{-1})$  for the corrosion of mild steel in concrete in NaCl 0.5M, t= 28 days at various concentrations of L<sub>1</sub> at different temperatures.

The entropy  $\Delta S_a$  and enthalpy  $\Delta H_a$  of activation were then determined using equation (15) which is the alternative formulation (called transition state) from (14) (Table 8)

$$i_{corr} = \frac{RT}{Nh} \exp\left(\frac{\Delta S_a}{R}\right) \exp\left(\frac{-\Delta H_a}{RT}\right) \quad (15)$$

where:

h: Plank's constant

N: Avogadro's number

The plot of  $\ln(i_{corr}/T) = f(T^{-1})$  is a straight line (Fig.13) and  $\Delta S_a = R (-b - \ln \frac{R}{Nh})$

The activation energy in the presence of different concentrations of  $L_1$  in the concrete is smaller than the activation energy of concrete without  $L_1$  which means that  $L_1$  has a chemisorption behavior [57, 64].

The endothermic nature of dissolving process of the steel is identified by the positive sign of the enthalpy  $\Delta H_a$  [64]. In our work  $\Delta H_a$  is negative reflecting the exothermic process of dissolving steel. The negative values of entropy  $\Delta S_a$  imply that the formation of activated complex in the determining rate step represents an association rather than dissociation. There is a decrease in disorder during transformation of the reactants into an activated complex [64].

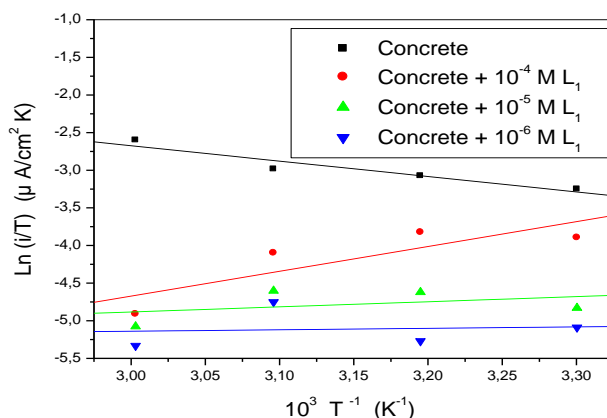


**Figure 13.**  $\ln(i_{corr}/T) = f(T^{-1})$  for the corrosion of mild steel in concrete in NaCl 0.5M, t= 28 days at various concentrations of  $L_1$  at different temperatures.

**Table 8.** Activation parameters for adsorption of  $L_1$  on mild steel surface.

Samples	$E_a(\text{kJmol}^{-1})$	$\Delta H_a(\text{kJmol}^{-1})$	$\Delta S_a(\text{Jmol}^{-1})$
Concrete	19.7	17	-168.7
Concrete + $10^{-4}$	-24.8	-27	-318.6
Concrete + $10^{-5}$	-3	-5.7	-255.1
Concrete + $10^{-6}$	1	-1.6	-245.1

### 3.5. MEB analysis

The morphology of steel surfaces in concrete in presence and absence of inhibitor in 0.5M NaCl was performed by SEM (Fig.14). As it is clearly seen from figure 14a, corroded surface was noted for inhibitor free solution. Moreover, some of concrete residuals were observed on the steel surface. The SEM image of steel surface in concrete containing inhibitor immersed even after 10 months in 0.5M

NaCl solution seems to be smoother and without cracks. The change in the steel surface due to the adsorption of inhibitor molecules is clearly shown in figure 14b. This confirms the results of electrochemical analysis results.

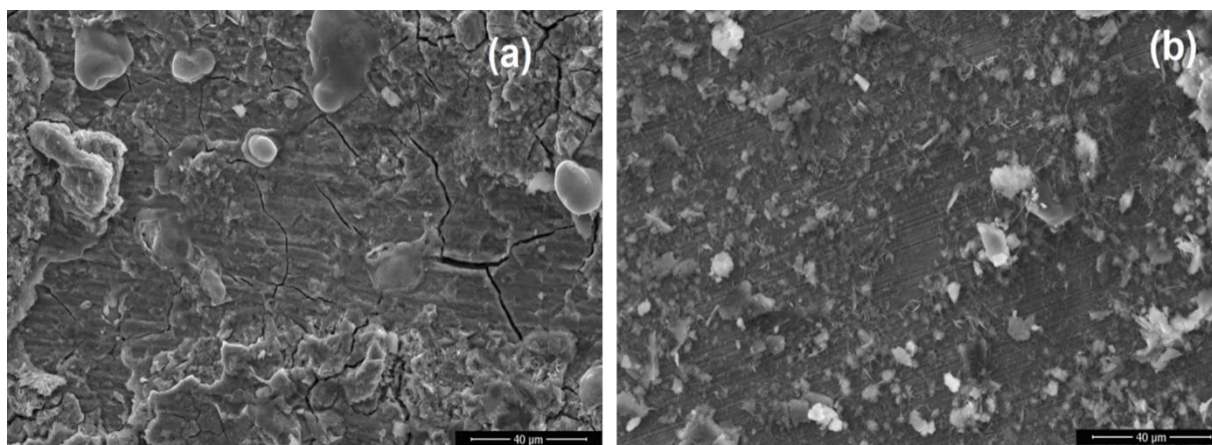


**Figure 14.** Micrographics of mild steel concrete without (a) and with  $L_1$   $10^{-6}M$  (b) after immersion in chloride environment of NaCl 0.5M,  $t= 10$  months.

### 3.6. Mechanical resistance (Flexural and compressive strengths)

The specimens are made only with concrete and without mild steel to see the effect of the addition of the inhibitor  $L_1$  dissolved in NaOH 0.1M on the mechanical strength of concrete. A good resistance of flexion and compression in the presence of lower concentration of  $L_1$  ( $10^{-6}M$ ) is observed (Table 9). The values of the flexural and compressive strengths do not change considerably varied. No important influence of the inhibitor on the flexural and compressive strengths of concrete was observed. This result leads to use the compound  $L_1$  safely in the concrete.

### 3.7. Theoretical study

The quantum chemical calculation method has been applied to investigate the influence of the electronic parameters and molecular structure on the protective power of  $L_1$ . The DFT technique was used to see concordance with experimental data. Figure 15 represents the Mullikan charges density, the optimized structure and the frontier molecular orbital density distributions of  $L_1$  obtained by the B3LYP/6-31G (d,p) method.

The quantum chemical parameters such as:  $E_{HOMO}$ ,  $E_{LUMO}$ ,  $\Delta E_{L-H}$ ,  $\mu$ ,  $\chi$ ,  $\eta$ ,  $\sigma$ ,  $\omega$  and  $\Delta N$  affect the inhibitory effectiveness [31]. These quantum chemical characteristics for the estimated structure of the neutral  $L_1$  in gas and aqueous phases (Table 10) were determined from equations (2) to (8).

**Table 9.** Flexural and compressive strengths of the samples at different immersion times.

Immersion time (Days)	Simple	Outside	Strength of Flexion (M.Pa)	Compressive strength (M.Pa)
2	Concrete		3.9	19
	Concrete + L <sub>1</sub> 10 <sup>-6</sup> M	NaCl 0.5M	3.7	19
	Concrete + L <sub>1</sub> 10 <sup>-5</sup> M		3.9	18
	Concrete + L <sub>1</sub> 10 <sup>-4</sup> M		3.8	17
28	Concrete		68	330
	Concrete + L <sub>1</sub> 10 <sup>-6</sup> M	NaCl 0.5M	73	333
	Concrete + L <sub>1</sub> 10 <sup>-5</sup> M		71	325
	Concrete + L <sub>1</sub> 10 <sup>-4</sup> M		68	325
90	Concrete		79	372
	Concrete + L <sub>1</sub> 10 <sup>-6</sup> M	NaCl 0.5M	78	361
	Concrete + L <sub>1</sub> 10 <sup>-5</sup> M		76	353
	Concrete + L <sub>1</sub> 10 <sup>-4</sup> M		66	355

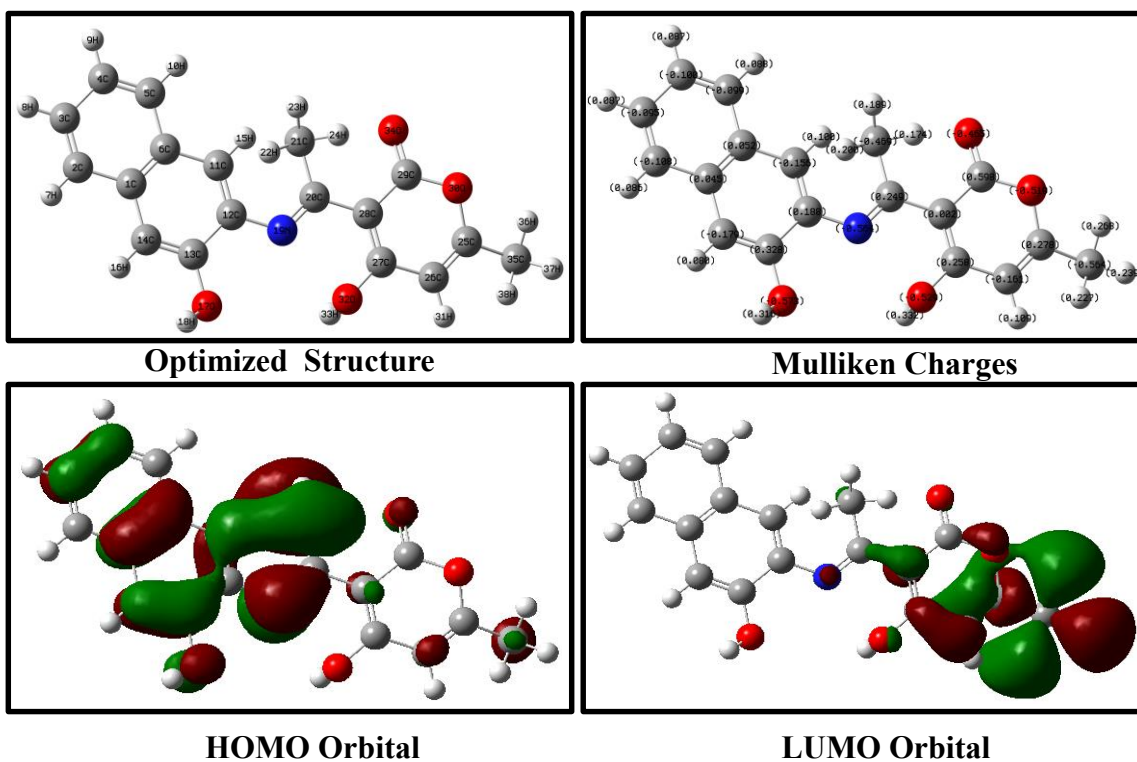


**Figure 15.** Optimized structure, Mullikan charges density and the HOMO and LUMO of L<sub>1</sub> given by the B3LYP/6-31(d,p).

**Table 10.** Quantum chemical parameters for L<sub>1</sub> in the gas and aqueous phase obtained by B3LYP/6-31G(d,p) basis set.

Quantum parameters	Gas phase	Aqueous phase
E <sub>tot</sub> (eV)	-28571.5	-28572.4
E <sub>Homo</sub> (eV)	-5.3	-5.5
E <sub>Lumo</sub> (eV)	-2.3	-1.9
ΔE <sub>GAP</sub> (eV)	3	3.6
μ(Debye)	5	6.4
η(eV)	1.5	1.8
σ	0.7	0.6
χ(eV)	3.8	3.7
ω	4.7	3.8
ΔN	1.1	0.9

The values of HOMO and LUMO energies and ΔE are in good concordance with the inhibitory power [28, 31]. Generally, if the ΔE and E<sub>LUMO</sub> decrease and the E<sub>HOMO</sub> increases, the inhibitors efficiency increases. An elevated value of E<sub>HOMO</sub> involves a stronger chemisorption leading to a higher inhibition behavior for the examined species. In another side, small E<sub>LUMO</sub> values indicate that the probability of the molecule to accept electrons increases. In this fact, the low value of ΔE can provide stronger chemisorption of the inhibitor molecules on the metal surface [25, 26]. This can be possible because removing electrons from HOMO needs a small energy. This confirms the obtained results and it is in a good agreement with the values of ΔN [25]. From table 10 one can see that the value of E<sub>HOMO</sub>=-5.3eV of L<sub>1</sub> confirms the high inhibitory power [31].

The formation of the covalent bonds between the inhibitor and the metal ion depends on the value of E<sub>LUMO</sub>. This later of E<sub>LUMO</sub> = -2.3eV indicates the easiness for this molecule to receipt electrons from the d orbital of the metal [27, 31]. The adsorption power of the inhibitor molecule on the metallic area is inversely proportional to the ΔE parameter. From table 10, it is clearly shown that L<sub>1</sub> has a low value of ΔE (3eV), which agrees with literature [27, 31]. The dipole moment (μ) influences the inhibitive ability of molecules [31]. It is directly proportional to the adsorption. Therefore, a quasi-substitution process occurs between molecules of L1 and water ones on the steel area, with desorption of water molecules from the metal. Thus, the inhibition process can be done. The value of μ<sub>inb</sub> (5Debye) (Table 10) is higher to μ<sub>H<sub>2</sub>O</sub> (1.88Debye) [28]. The low energy gap and the high value of dipole moment imply the electrons exchange from the inhibitor to the metallic area. This could be done when the adsorption process occurs on the carbon steel surface. The measured absolute hardness and softness affect the molecular stability and molecular reactivity. A hard molecule is characterized by a large energy gap and a small one distinguishes a soft molecule. The reactivity of the hard molecules is less than that of the soft ones: it is difficult to the hard molecules to give electrons to an acceptor. The adsorption occurs in the part of the molecule where σ is high [28]. In this study, the inhibition rate will be enhanced because of the low value of the global hardness (1.5eV) and the high value of the global softness (0.7) (Table

10). Such results corroborate with the bibliography [28, 65]. Thus, the value of the energy gap (3) being low confirms  $L_1$ 's reactivity with metal atoms.

The inhibitory power is also influenced by the value of the electrophilicity index ( $\omega$ ). The inhibitor effectiveness increases with the decrease of the  $\omega$  value. The value of  $\omega$  (4.7) agrees with the high value of the protection rate [28]. The elevating in the electron transfer ability to the metal surface justifies the increase of the chemisorption and the inhibition power [66]. Consequently, if the strength of the coordinate bond between iron and inhibitor enhances, the inhibiting action of corrosion due to chemisorption increases. The corrosion inhibition power of  $L_1$  being high reflects the good inhibition efficiency resulting from the good chemical adsorption of this Schiff base. This fact is explained by the high number of transferred electrons (1.1). From table 10, the low electrophilicity  $\omega = 4.7$  agree with the studied inhibitor behavior. It is also noticed that  $\Delta N$  is positive and less than 3.6 [28, 65]. The inhibitor can donate electrons to iron to form coordinate bonds and give rise consequently to adsorption inhibitive layers against corrosion. The electronegativity value of the inhibitor molecule is equal to 3.8. This electronegativity value ( $\chi=3.8$ ) being inferior to that of iron suggests an exchange of electron between the high occupied molecular orbital of the inhibitor (HOMO) and the unoccupied 3d orbitals of iron. This electron transfer is more probable than that from the occupied 4s orbital of Fe to the low unoccupied molecular orbital (LUMO) of the inhibitor. The high electronegativity of the nitrogen atom over the carbon one as well as the existence of a more electronegative oxygen atom in the dehydroacetic acid and hydroxyl groups explains the low value of  $\chi$ . So, the electron flow from the studied Schiff base promotes high adsorption and consequently an elevate inhibition efficiency [31].

In order to localize the electrophilic and nucleophilic sites, the Molecular Electrostatic Potential (MEP) is employed [67] using the optimized geometry of the  $L_1$ . Figure 16 represents the mapped electron density surface of  $L_1$ . The nucleophilic actives regions are colored in light blue and blue when the red and yellow colors in MEP map indicate the electrophilic active ones. The positively charged and negatively charged regions are presented by the yellow and red color lines respectively. It is clear from figure 16 that the heteroatoms and the conjugated double bonds localize the more electron rich regions. The electrophilic active sites are centred at oxygen atoms (O17, O32 and O34), nitrogen one (N19) and the conjugated double bonds of naphthyl group. The 4-hydroxy-3- [1- (3-hydroxy-naphthalen-2-ylimino)-ethyl] -6-methyl-pyran-2-one studied and promoted can chelate the surface of mild steel by transferring electrons of dihydroacetic acid and hydroxy-naphthyls to the iron atoms by forming covalent bonds through a chemical adsorption mechanism. In the corrosion protecting process by this molecule, the nucleophilic reactions occur with heteroatoms and electrons of the conjugated double bonds. Figure 16 show clearly that HOMO energy level of  $L_1$  is mostly distributed over the hydroxyl aminonaphthyl group, oxygen (O32, O34) of the dehydroxyacetic acid moiety, the oxygen and the nitrogen (O17, N19) of the hydroxyl aminonaphthyl group.

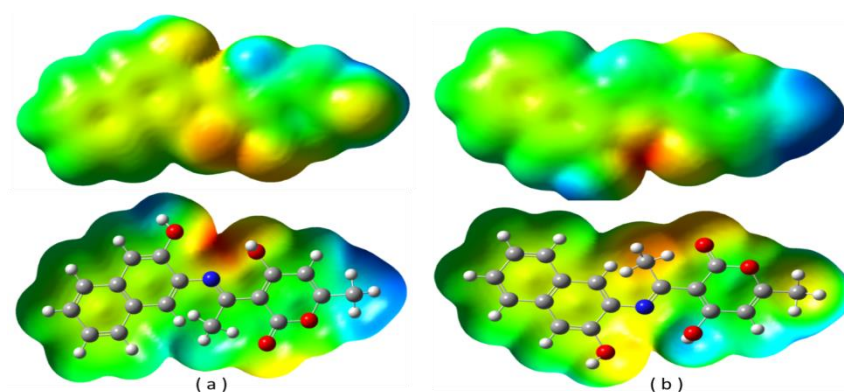


**Figure 16.** MEP map and counter plot of L<sub>1</sub> (a) Front view and (b) Rear view.

In order to evaluate the method how the atomic displacement affects the electronic structure charge Mulliken were used. The results were presented on the atoms in the optimized structure (Fig.15). The effective atomic charges from Mulliken populations presented in table 11 show that N19, O30, O32 and O34 as well as some carbon atoms, wear negative charges in L<sub>1</sub>. These atoms are the more negative charge centers that could give electrons to the Fe atoms in order to coordinate it, and the positive charge centers that can accept electrons from 3d orbital of the Fe atoms to form feedback bond, thus further strengthening the interaction of inhibitor and Fe surface. This implies that L<sub>1</sub> has potential heteroatoms that can be adsorbed in positive centers on the metallic surface through a donor-acceptor type reaction [27].

**Table 11.** Mulliken atomic charges of the L<sub>1</sub>.

Atom	Gas phase		Aqueous phase	
	Mulliken charges	NBO charges	Mulliken charges	NBO charges
C <sub>1</sub>	0.045	-0.045	0.027	-0.055
C <sub>2</sub>	-0.108	-0.218	-0.123	-0.224
C <sub>3</sub>	-0.095	-0.235	-0.111	-0.240
C <sub>4</sub>	-0.101	-0.239	-0.116	-0.244
C <sub>5</sub>	-0.099	-0.213	-0.115	-0.221
C <sub>6</sub>	0.052	-0.041	0.039	-0.050
H <sub>7</sub>	0.086	0.237	0.111	0.250
H <sub>8</sub>	0.087	0.238	0.107	0.250
H <sub>9</sub>	0.087	0.239	0.108	0.249
H <sub>10</sub>	0.088	0.238	0.111	0.249
C <sub>11</sub>	-0.156	-0.292	-0.171	-0.295
C <sub>12</sub>	0.188	0.119	0.176	0.109
C <sub>13</sub>	0.328	0.333	0.314	0.320
C <sub>14</sub>	-0.179	-0.299	-0.187	-0.295
H <sub>15</sub>	0.100	0.277	0.119	0.280

H <sub>16</sub>	0.080	0.237	0.115	0.255
O <sub>17</sub>	-0.573	-0.706	-0.600	-0.727
H <sub>18</sub>	0.316	0.493	0.344	0.514
N <sub>19</sub>	-0.564	-0.494	-0.587	-0.521
C <sub>20</sub>	0.249	0.299	0.246	0.305
C <sub>21</sub>	-0.469	-1.074	-0.544	-1.106
H <sub>22</sub>	0.200	0.353	0.213	0.357
H <sub>23</sub>	0.189	0.372	0.226	0.393
H <sub>24</sub>	0.174	0.380	0.188	0.384
C <sub>25</sub>	0.278	0.405	0.285	0.408
C <sub>26</sub>	-0.161	-0.405	-0.170	-0.406
C <sub>27</sub>	0.258	0.404	0.266	0.412
C <sub>28</sub>	0.002	-0.251	-0.003	-0.266
C <sub>29</sub>	0.598	0.801	0.607	0.811
O <sub>30</sub>	-0.519	-0.516	-0.521	-0.515
H <sub>31</sub>	0.109	0.251	0.142	0.269
O <sub>32</sub>	-0.529	-0.701	-0.560	-0.723
H <sub>33</sub>	0.332	0.513	0.347	0.525
O <sub>34</sub>	-0.465	-0.570	-0.507	-0.609
C <sub>35</sub>	-0.564	-1.210	-0.627	-1.214
H <sub>36</sub>	0.268	0.459	0.293	0.467
H <sub>37</sub>	0.239	0.432	0.292	0.462
H <sub>38</sub>	0.227	0.431	0.266	0.446

The results of Natural bonding orbital (NBO) analysis were summarized in table 11. It is demonstrated that nitrogen, oxygen and some carbon atoms of hydroxyl aminonaphthyl and dihydroacetic rings of L<sub>1</sub> are negatively charged. The calculated characteristics in gas phase as well as in the aqueous one are not different (Table 10) except the value of  $\mu$ . The increase of this last parameter is explained by the polarization of the inhibitor molecules caused by the molecule-solvent interactions. These results concord with the low value of gap energy, and permit us to conclude that L<sub>1</sub> has a good reactivity and this implies high inhibition efficiency.

#### 4. CONCLUSION

An original tridentate Schiff base and eco-friendly inhibitor (L<sub>1</sub>) namely: 4-hydroxy-3-[1-(3-hydroxy-naphthalen-2-ylimino)-ethyl]-6-methyl-pyran-2-one was chemically synthesized and characterized by usual methods. A crystallographic structure of this heterocyclic compound was identified. Inhibiting property of this organic compound is examined against corrosion of mild steel enrobed with concrete in NaCl 0.5M solution. Electrochemical results obtained for L<sub>1</sub>, with linear potentiodynamic method and impedance spectroscopy show important protective characteristics against the corrosion of the concrete rebars. The inhibition effectiveness is optimum for 10<sup>-6</sup>M L<sub>1</sub>.

The results of potentiodynamic polarization measurements show that L<sub>1</sub> is a cathodic inhibitor. The protection mechanism follows spontaneous adsorption according to Langmuir isotherm. The

thermodynamic adsorption parameters confirm that L<sub>1</sub>'s adsorption mechanism follows a chemisorption process. The electrochemical results were confirmed by SEM analysis. The theoretical results obtained by the quantum chemical study agree with the experimental ones.

Also, MEP analysis indicates that the appropriate heteroatoms for the interaction in the inhibition of the corrosion process are the oxygen and nitrogen atoms. The sites N19, O17, O32 and O34 are most favorable for electrophilic reaction. Consequently, the probable atoms in this structure to coordinate iron are these last heteroatoms. The NBO and MEP results are in good concordance.

The mechanical study performed reveals a good resistance of flexion and compression in the presence of lower concentration of L<sub>1</sub> (10<sup>-6</sup>M).

In summary, this investigation confirmed the good and high inhibitory power of this new tridentate Schiff base towards corrosion of mild steel in concrete. This organic inhibitor is promoted to the field of civil engineering.

#### ACKNOWLEDGEMENTS

The authors gratefully acknowledge the financial support from the Algerian Ministry of Higher Education and Scientific Research. The authors would like to thank Professors Jean Paul Guisselbrecht from Laboratoire d'Electrochimie et de Chimie Physique du Corps Solide ULP Strasbourg France and Professors Mehmet Erbil and Tunç Tüken from Faculty of Science and Letters Chemistry Department Çukurova University Turkey for helpful.

#### References

1. M. Osial and D. Wiliński, *J. Build. Chem.*, 1 (2016) 42.
2. B. Huet, V. L'Hostis, F. Miserque and H. Idrissi, *Electrochim. Acta*, 51 (2005) 172.
3. V. Kumar, R. Singh and M.A. Quraishi, *J. Mater. Environ. Sci.*, 4 (5) (2013) 726.
4. R.R. Moreira, T.F. Soares and J. Ribeiro, *Adv. Chem. Eng. Sci.*, 4 (2014) 503.
5. A.S. Abdulrahman, M. Ismail and M.S. Hussain, *Sci. Res. Essays*, 6 (20) (2011) 4152.
6. M. Ormellese, L. Lazzari, S. Goidanich, G. Fumagalli and A. Brenna, *Corros. Sci.*, 51 (2009) 2959.
7. J. Abdul Bari, M. Velumani and B. Monisha, *Int. J. Eng. Tech. Sci. Res.*, 4 (1) (2017) 1.
8. M. Criado, C. Monticelli, S. Fajardo, D. Gelli, V. Grassi and J.M. Bastidas, *Constr. Build. Mater.*, 35 (2012) 30.
9. M. Pandiarajan, S. Rajendran, J. Sathiyabama, J. Lydia Christy, J. Jeyasundari and P. Prabhakar, *Eur. Chem. Bull.*, 2 (1) (2013) 1.
10. T.A. Söylev and M.G. Richardson, *Constr. Build. Mater.*, 22 (2008) 609.
11. S. Sawada, C.L. Page and M.M. Page, *Corros. Sci.*, 47 (2005) 2063.
12. E. Rakanta, Th. Zafeiropoulou and G. Batis, *Constr. Build. Mater.*, 44 (2013) 507.
13. J. Kubo, Y. Tanaka, C.L. Page and M.M. Page, *Constr. Build. Mater.*, 39 (2013) 2.
14. G. Mangaiyarkarasi and S. Muralidharan, *Procedia Eng.*, 86 (2014) 615.
15. J.O. Okeniyi, *J. Assoc. Arab Univ. Basic Appl. Sci.*, 20 (2016) 39.
16. A.N. Ababneh, M.A. Sheban and M.A. Abu-Dalo, *J. Mater. Civ. Eng.*, 24 (2012) 141.
17. C.A. Jeyasehar and V. Madhavan, *AJCE(bhrc)*, 15 (3) (2014) 363.
18. U.M. Angst, M. Büchler, J. Schlumpf and B. Marazzani, *Mater. Struct.*, 49 (7) (2016) 2807.
19. J. Meyer, *Brian Cherry International Concrete Symposium* 12 (2017) 1.
20. O.S.B. Al-Amoudi, M. Maslehuddin, A.N. Lashari and A. Almusallam, *Cem. Concr.*

- Comp., 25 (2003) 439.
21. J.O. Okeniyi, A.P.I. Popoola and C.A. Loto, *Energy Procedia*, 119 (2017) 972.
  22. A.A. Gürten, E. Bayol, K. Kayakirilmaz and M. Erbil, *Steel and Composite Structures*, 9 (1) (2009) 77.
  23. M.V. Diamanti, E.A. Pérez Rosales, G. Raffaini, F. Ganazzoli, A. Brenna, M. Pedferri and M. Ormellese, *Corros. Sci.*, 100 (2015) 231.
  24. S. Kaya, C. Kaya, L. Guo, F. Kandemirli, B. Tüzün, İ. Uğurlu, L.H. Madkour and M. Saraçoğlu, *J. Mol. Liquids*, 219 (2016) 497.
  25. A.S. Fouda, G.Y. Elewady, K. Shalabi and H.K. Abd El-Aziz, *Rsc. Adv.*, 5 (2015) 36957.
  26. L. Feng, H. Wang and F. Wang, *Electrochim. Acta*, 58 (2011) 427.
  27. L.H. Madkour and S.K. Elroby, *J.C.S.E.*, 17 (4) (2014) 1.
  28. L.H. Madkour, S. Kaya, C. Kaya and L. Guo, *J. Taiwan. Inst. Chem. Eng.*, 68 (2016) 461.
  29. Y. Wang and Y. Zuo, *Corros. Sci.*, 118 (2017) 24.
  30. L.H. Madkour and U.A. Zinhome, *J.C.S.E.*, 13 (34) (2010) 1.
  31. L.H. Madkour and S.K. Elroby, *Int. J. Ind. Chem.*, 6 (2015) 165.
  32. A.D. Becke, *J. Chem. Phys.*, 98 (1993) 5648.
  33. C. Lee, W. Yang and R.G. Parr, *Phys. Rev. B*, 37 (2) (1988) 785.
  34. M. Frisch, G. Trucks, H. Schlegel, G. Scuseria, M. Robb, J. Cheeseman, G. Scalmani, V. Barone, B. Mennucci and G. Petersson, Gaussian 09, Revision A. 1, *Gaussian Inc.*, Wallingford, CT. (2009).
  35. R. Dennington, T. Keith and J. Millam, GaussView, Shawnee Mission, KS: Semichem, *Incorporated Company Officers* (2009).
  36. R.G. Parr and R.G. Pearson, *J. Am. Chem. Soc.*, 105 (12) (1983) 7512.
  37. A.Y. Musa, A.A.H. Kadhun, A.B. Mohamed and M.S. Takriff, *Mater. Chem. Phys.*, 129 (2011) 660.
  38. F. Zhang, Y.M. Tang, Z. Cao, W. Jing, Z. Wu and Y. Chen, *Corros. Sci.*, 61 (2012) 1.
  39. A. A. Osowole, *E- J. Chem.*, 5 (1) (2008) 130.
  40. W. J. Geary, *Coord. Chem. Rev.*, 7 (1971) 81.
  41. V.A. Shelke, S.M. Jadhav, S.G. Shankarwar and T.K. Chondhekar, *J. Chem. Sci. Tech.*, 2 (2) (2013) 61.
  42. S.M. Emam, A.S. El-Tabl, H.M. Ahmed and E.A. Emad, *Arab. J. Chem.*, 10 (2017) S3816.
  43. R.K. Pawar, M.A. Sakhare and B.R. Arbad, *Int. J. Chem. Sci.*, 14 (4) (2016) 2575.
  44. A. Garay, R. Abonia, J. Cobo and C. Glidewell, *Acta Cryst.*, C70 (2014) 210.
  45. G.M. Sheldrick, *Acta Cryst.*, A64 (2008) 112.
  46. B.V. Nonius, COLLECT Delft, The Netherlands, (1998).
  47. A.L. Spek, *Acta Cryst.*, D65 (2009) 148.
  48. A. Djedouani, A. Bendaas, S. Boufas, M. Allain, G. Bouet and M. Khan, *Acta Cryst.*, E63 (2007) o1271.
  49. P. Balamurugan, R. Jagan, K. Parthiban, G. Rajagopal, and K. Sivakumar, *Anal. Sci.*, 24 (2008) x295.
  50. F. Benghanem, S. Keraghel, S. Chahmana, A. Ourari and L. Brelot, *Acta Cryst.*, E68 (2012) o2189.
  51. A. Özek, S. Yüce, C. Albayrak, M. Odabaşoğlu and O. Büyükgüngör, *Acta Cryst.*, E60 (2004) o828.
  52. M. Odabaşoğlu, C. Albayrak and O. Büyükgüngör, *Acta Cryst.*, E60 (2004) o142.
  53. Ö. Güngör and P. Gürkan, *Spectrochim. Acta*, A77 (2010) 304.
  54. S. Chahmana, F. Benghanem, S. Keraghel and A. Ourari, *Acta Cryst.*, E70 (2014) o107.
  55. J. Liu, D. Zhao, J. Cai, L. Shi and J. Liu, *Int. J. Electrochem. Sci.*, 11 (2016) 8758.

56. J.O.M. Bockris and S. Srinivasan, *Electrochim. Acta*, 9 (1964) 31.
57. L. Toukal, S. Keraghel, F. Benghanem and A. Ourari, *Int. J. Electrochem. Sci.*, 13 (2018) 951.
58. M.A. Hegazy, E.M.S. Azzam, N.G. Kandil, A.M. Badawi and R.M. Sami, *J. Surfact. Deterg.*, 19 (2016) 861.
59. G. Siğircık, T. Tüken and M. Erbil, *Corros. Sci.*, 102 (2016) 437.
60. B. Xu, W. Yang, Y. Liu, X. Yin, W. Gong and Y. Chen, *Corros. Sci.*, 78 (2014) 260.
61. G. Kılınççeker and C. Menekşe, *Prot. Met. Phys. Chem.*, 51 (2015) 659.
62. M. Cafferty and E. Hackerman, *J. Electrochem. Soc.*, 119 (8) (1972) 999.
63. F.M. Donahue and K. Nobe, *J. Electrochem. Soc.*, 112 (9) (1965) 886.
64. S.A. Wanees, A.B. Radwan, M.A. Alsharif and S.M.A. Haleem, *Mater. Chem. Phys.*, 190 (2017) 79.
65. S.Kr. Saha, A. Dutta, P. Ghosh, D. Sukul and P. Banerjee, *Phys. Chem. Chem. Phys.*, 00 (2013) 1.
66. I. Lukovits, E. Klaman and F. Zucchi, *Corrosion*, 57 (2001) 3.
67. N. Okulik and A.H. Jubert, *Internet Electron. J. Mol. Des.*, 4 (2005) 17.

© 2018 The Authors. Published by ESG ([www.electrochemsci.org](http://www.electrochemsci.org)). This article is an open access article distributed under the terms and conditions of the Creative Commons Attribution license (<http://creativecommons.org/licenses/by/4.0/>).